

TRACE: Transform Aggregate and Compose Visiolinguistic Representations for Image Search with Text Feedback

Surgan Jandial^{*†3}, Ayush Chopra^{*‡2}, Pinkesh Badjatiya^{*1}, Pranit Chawla^{†4}, Mausoom Sarkar¹, Balaji Krishnamurthy¹

¹ Media and Data Science Research Lab, Adobe

² Massachusetts Institute of Technology

³ Indian Institute Of Technology, Hyderabad

⁴ Indian Institute Of Technology, Kharagpur

Abstract

The ability to efficiently search for images over an indexed database is the cornerstone for several user experiences. Incorporating user feedback, through multi-modal inputs provide flexible and interaction to serve fine-grained specificity in requirements. We specifically focus on text feedback, through descriptive natural language queries. Given a reference image and textual user feedback, our goal is to retrieve images that satisfy constraints specified by both of these input modalities. The task is challenging as it requires understanding the textual semantics from the text feedback and then applying these changes to the visual representation. To address these challenges, we propose a novel architecture *TRACE* which contains a hierarchical feature aggregation module to learn the composite visio-linguistic representations. *TRACE* achieves the SOTA performance on 3 benchmark datasets: FashionIQ, Shoes, and Birds-to-Words, with an average improvement of at least $\sim 5.7\%$, $\sim 3\%$, and $\sim 5\%$ respectively in R@K metric. Our extensive experiments and ablation studies show that *TRACE* consistently outperforms the existing techniques by significant margins both quantitatively and qualitatively.

1 Introduction

The global retail e-commerce market was valued at \$4.25 trillion in 2019. Furthermore, recent social-cultural transformations have necessitated growth with renewed estimates that project increase at a compound annual growth rate (CAGR) of 9.4% from 2020 to 2027. Consequently, there is significant interest in providing smart, intuitive experiences for online commerce including fine-grained tagging (Zhou and Lin 2016; Ak et al. 2018), virtual try-on (Jandial et al. 2020, 2019b,a; Han et al. 2018), product recommendations (McAuley et al. 2015; Tanmay and Ayush 2019) and image search (Gordo et al. 2016; Bell and Bala 2015; Chopra et al. 2019). In particular, the ability to search for product images over an indexed catalog is a fundamental task that serves as a cornerstone for several allied user experiences.

*equal contribution

†work done as part of Adobe MDSR internship program

‡work done while at Adobe

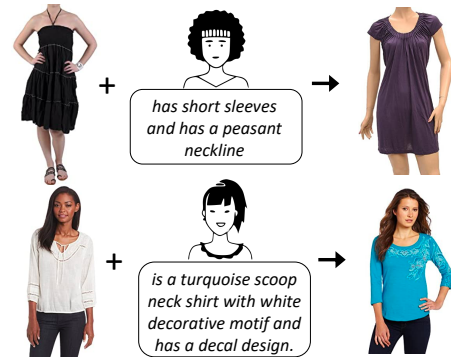


Figure 1: Given a reference image and the descriptive feedback provided by the user, we retrieve the results which not only resemble the original image but also incorporate the changes as requested in the user query

The most ubiquitous frameworks in image search either take image or text as input query to search for relevant items (Noh et al. 2017; Gordo et al. 2016). However, a key limitation of these frameworks is the infeasibility to capture intricate user requirements which cannot be precisely encapsulated with a single image or a combination of keywords. Correspondingly, several interactive paradigms are being explored which can incorporate user feedback to help tailor retrieved results to specific user intentions. These interactions involve refining upon a reference query image through feedback in form of spatial layouts (Mai et al. 2017), scene-graphs (Johnson et al. 2015; Ramnath et al. 2019; Wang et al. 2020) or relative and certain attributes (Yu and Grauman 2019; Han et al. 2017; Zhao et al. 2017; Ma et al. 2020b). Furthermore, text feedback via natural language queries presents immense promise in providing more flexibility to the user for interactive image search (Guo et al. 2018). In this work, we focus on incorporating diverse, unconstrained natural language descriptions as feedback for interactive image search with the specific task denoted as text conditioned image retrieval (*TCIR*). Formally, given a reference image as input and a support text description as feedback, *TCIR* is concerned with retrieving the best matching images that satisfying similarity constraints imposed by

both components of the multi-modal input.

Learning joint image-text representations is key to several popular tasks such as language grounding (Tellex et al. 2011; Misra et al. 2015; Sinha et al. 2019), captioning (Karpathy and Fei-Fei 2015), Visual Question Answering (VQA) (Antol et al. 2015; Patro and Namboodiri 2018), visual reasoning (Sarafianos, Xu, and Kakadiaris 2019; Xu et al. 2020; Zhang et al. 2020), etc. These tasks use the text input to primarily guide image saliency and are interested in addressing the *where-to-look* problem. Tasks like VQA focus on incorporating the global text semantics to localize objects in an image (Singh et al. 2019; Sarafianos, Xu, and Kakadiaris 2019; Xu et al. 2020; Zhang et al. 2020). Correspondingly, research in the domain has introduced several attention mechanisms (Yu et al. 2017) to encode textual context in visual representations. Although novel and effective, these techniques are inadequate for our task.

The task of text-conditioned image retrieval is more involved and requires learning multi-modal representations that can simultaneously address “*where-to-look*” and “*how-to-change*”. In particular, our work focuses on natural language queries of variable length as text feedback. Major challenges are concerned with accommodating the multiple, spatially, and semantically disentangled, visual transformations that a user may request. Figure 1 shows some of the examples relevant to our task. As in Row 1, a user can parallelly propose edits in both shape and style (color, length, pattern, geometry) of multiple distinct regions (collar, sleeves, neckline). For eg, *with short sleeves and peasant neckline*. Also, as in Row 2, text descriptions can request multi-granular, local, and global semantic edits. For eg, *is a turquoise scoop neck tshirt with white decorative motif and has a decal design*.

In this work, we focus on learning image-text representations that can incorporate textual cues with multiple fine-grained semantic edits with visual representations. Recent works have shown that ConvNets learn image features hierarchically with increasing abstractions across the pyramidal levels (LeCun, Bengio, and Hinton 2015; Zeiler and Fergus 2014). Consequently, we focus on utilizing this granular feature abstraction for attentional learning of image features with text queries. We introduce a pyramidal attention and fusion module consisting of three key phases: **TR**ansform **A**ggregate **C**ompose (or **TRACE**). First, granular visual representations are *semantically* transformed through textual co-attention. Next, transformed features across the pyramid are hierarchically *aggregated* to generate a coarse visio-linguistic representation. This aggregated representation is utilized as a residual offset and *composed* with the textual features to generate a multi-modal compositional embedding. Further, discriminative and consistency objectives are used to reinforce the utilization of semantic information in the composed embedding.

Our contributions can be summarized as follows,

- We introduce *TRACE*, a framework to systematically *transform, aggregate* and *compose* visio-linguistic embeddings for text conditioned image retrieval, and use discriminative and consistency objectives to regularize representation learning.

- We perform detailed quantitative and qualitative analysis on 3 benchmark datasets with varying lengths of natural language queries and consistently achieve SOTA results.
- We also conduct extensive ablative studies to analyze the impact of each component of the proposed framework.

2 Related Work

Product Search and Image Retrieval has attracted significant research interest owing to its diverse practical applicability (Halawani et al. 2006; Noh et al. 2017). Conventionally, search has focus on using uni-modal (image or text) queries to retrieve visually similar (Chopra et al. 2019; Bell and Bala 2015) or compatible (Singhal et al. 2020) images. More recently, we have witnessed a surge in interactive multi-modal techniques that incorporates user feedback to navigate visual search. The user interactions can manifest in form of attributes (Ak et al. 2018; Zhao et al. 2017; Ma et al. 2020b), spatial layouts (Mai et al. 2017; Barman and Shah 2019; Ma et al. 2020a), sketches (Yu et al. 2016; Sangkloy et al. 2016; Dutta and Biswas 2020; Ghosh et al. 2019), scene-graph (Johnson et al. 2015; Rammath et al. 2019; Wang et al. 2020) and text descriptions (Vo et al. 2019; Chen, Gong, and Bazzani 2020; Guo et al. 2018). Owing to the ubiquity of text queries in existing search engines and their flexibility of articulation, using textual guidance can facilitate fine-grained specificity in user queries. In this work, we pursue visual search with textual feedback and propose a framework that efficiently handles unconstrained natural language descriptions of varying lengths.

Visiolinguistic Representation Learning involves jointly processing image and text inputs to learn unified multi-modal embeddings. This is central to several *vision-to-language* tasks such as VQA (Antol et al. 2015; Patro and Namboodiri 2018; Yu et al. 2019), Image-Text Matching (Sarafianos, Xu, and Kakadiaris 2019; Xu et al. 2020; Zhang et al. 2020), language grounding (Tellex et al. 2011; Sinha et al. 2019; Misra et al. 2015) which use the text input to primarily address the problem of “*where to look*” in the image. Earlier research has proposed various attention mechanisms to generate a coarse visual fixation. Other self-attention and co-attention techniques have been developed to learn intra-modal and inter-modal latent attention (Lee et al. 2018; Gao et al. 2019). Here, we focus on obtaining Visio-linguistic embeddings for the task of text-based image retrieval, which involves the need for fine-grained spatial/semantic co-attention to jointly addressing “*how to change*” along-with “*where to look*”. To get to this goal, we introduce a hierarchical co-attention scheme that learns to aggregate Visio-linguistic attention across multiple visual granularities. Our proposed approach is independent of pre-trained object detectors (Ren et al. 2015; Girshick 2015) and generalizes well to fine-grained visual search with diverse natural language queries.

Text Conditioned Image Retrieval can be visualized as learning a composite representation of an image and text. Although CNNs inherently learn the composition of visual

parts, they can not efficiently compose visual representations and natural-language semantics. TIRG (Vo et al. 2019) introduced a residual gating operation to fuse latent image and text embeddings, and VAL (Chen, Gong, and Bazzani 2020) concatenates the text embedding at multiple layers of the image CNN to extract the composite representations. We introduce a pyramidal gated fusion mechanism exploiting the CNNs hierarchical visual representations across varying abstractions (LeCun, Bengio, and Hinton 2015; Zeiler and Fergus 2014). Our method generates granular Visio-linguistic embeddings and leverages their coarse hierarchy to learn the final compositional representation.

3 Approach

Given a *Query Image* (I_q) and the *Support Text Description* (D_t), our training objective is to learn a composite feature embedding that aligns with the *Target Image* (I_t) embedding. First, we encode the Query Image with an *Image Encoder*, generating the multi-scale visual embeddings and then the Support Text with a *Text Encoder*, generating the textual feature representation. Then we *Transform, Aggregate* and *Compose* the features from multiple scales with modules described in detail in Sections 3.2, 3.3 and 3.4 to obtain a composite multi-modal representation. All components are jointly optimized using a combination of loss functions (explained in Section 3.5) specifically designed to regularize the visual and textual features when learning composite embeddings. Figure 2 provides the framework overview for *TRACE*.

3.1 Representing Image and Text

Image Encoder. To obtain a discriminative representation of the image we use a standard convolutional neural network (CNN). Since CNNs encode visual concepts with increasing abstraction over the multiple layers, we hierarchically extract multiple feature maps from the CNN to encapsulate information across different granularities. Concretely, the resultant visual feature pyramids F_q and F_t for the query and the target image respectively can be represented as,

$$\begin{aligned} F_q &= \{V_q^1, V_q^2, \dots, V_q^L\} = \phi_{\text{CNN}}(I_q) \\ F_t &= \{V_t^1, V_t^2, \dots, V_t^L\} = \phi_{\text{CNN}}(I_t) \end{aligned} \quad (1)$$

Here, I_q and I_t represent the query and target images respectively; F_q and F_t the feature pyramids and V_q^ℓ represents the ℓ^{th} feature map from the L levels of the feature pyramid. Throughout the text, we refer to any level in the feature pyramid as $\ell \in [1, L]$.

Text Encoder. Here, we use a GRU (Cho et al. 2014) followed by L parallel fully connected layers to generate L number of text embeddings corresponding to the visual feature map at each scale.

Given the support text D_t with a maximum of N words, we perform text tokenization and use the obtained words as input to obtain a sequence of word-level embedding features $F_{\text{word}} \in \mathbb{R}^{1 \times 768}$ which are then passed through a GRU to

obtain the support text feature $F_{\text{sent}} \in \mathbb{R}^{1 \times 1024}$ as

$$F_{\text{sent}} = \text{GRU}([F_{\text{word}}^1, F_{\text{word}}^2, \dots, F_{\text{word}}^N]) \quad (2)$$

The textual features T^ℓ at any level ℓ are then computed using,

$$T^\ell = \begin{cases} F_{\text{sent}}, & \text{if } \ell = 1 \\ \Omega_\ell(F_{\text{sent}}), & \text{otherwise} \end{cases} \quad \forall \ell \in [1, L] \quad (3)$$

where Ω_ℓ denotes a linear projection layer for a level ℓ .

3.2 SFT: Semantic Feature Transformation

After we obtain the image features V_q^ℓ and the textual features T^ℓ at any level ℓ , we transform the features to project them in a more coherent feature space.

Formally, given a visual feature map of the query image $V_q^\ell \in \mathbb{R}^{C_\ell \times H_\ell \times W_\ell}$ and the corresponding text embedding $T^\ell \in \mathbb{R}^{C_\ell}$, this module learns an attended image-text embedding O^ℓ which encodes information from both the modalities. We now provide the steps of the transformation operations below.

Attentional Visual Transformation: When learning joint visio-linguistic representations, capturing apriori long-range contextual relationships within the visual embedding (V_q^ℓ) helps in enhancing representational capabilities. To adaptively aggregate the spatial context, we thus leverage a positional attention mechanism (Zhang et al. 2019; Fu et al. 2019) to transform V_q^ℓ into volumetric representation $\bar{V}_q^\ell \in \mathbb{R}^{C_\ell \times H_\ell \times W_\ell}$. For this, V_q^ℓ is passed through parallel convolutional layers (denoted by $\Theta_q, \Theta_k, \Theta_v$) and then the obtained volume is reshaped to obtain new query and key feature maps denoted by $(Q^\ell, K^\ell) \in \mathbb{R}^{C_\ell \times N_\ell}$, where $N_\ell = H_\ell \times W_\ell$.

$$Q^\ell = \Theta_q(V_q^\ell), \quad K^\ell = \Theta_k(V_q^\ell), \quad V^\ell = \Theta_v(V_q^\ell) \quad (4)$$

Next, a spatial attention map is calculated by performing matrix multiplication between transpose of Q^ℓ and K^ℓ followed by softmax.

$$A_{\text{self}}^\ell = \text{softmax}(Q^{\ell T} K^\ell) \quad (5)$$

We now generate an intermediate representation E^ℓ by performing matrix multiplication of V_q^ℓ with the spatial attention map A_{self}^ℓ . Finally, the transformed attentive visual feature map is obtained as,

$$\begin{aligned} E^\ell &= V^\ell A_{\text{self}}^{\ell T} \\ \bar{V}_q^\ell &= \gamma * E^\ell + V_q^\ell \end{aligned} \quad (6)$$

where γ is a learnable scalar parameter.

The obtained feature vector \bar{V}_q^ℓ encodes the global visual information along with selectively aggregated spatial context which improves the semantic consistency in the representation.

Visiolinguistic Pooling: The learnt attentive visual representation \bar{V}_q^ℓ is now used to obtain the joint image-text features. For this, \bar{V}_q^ℓ is convolved with the corresponding

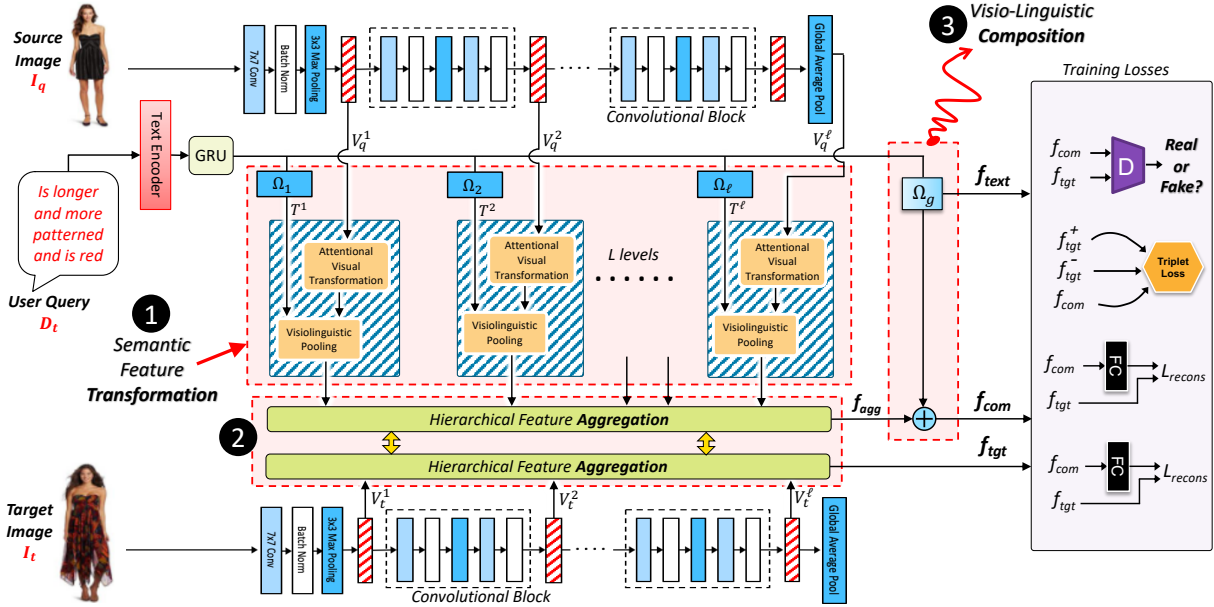


Figure 2: An overview of our proposed *TRACE* framework. We highlight the 3 main components in the figure: (1) **Semantic Feature Transformation** module, (2) the **Hierarchical Feature Aggregation** module and (3) the **Visio-Linguistic Composition** module.

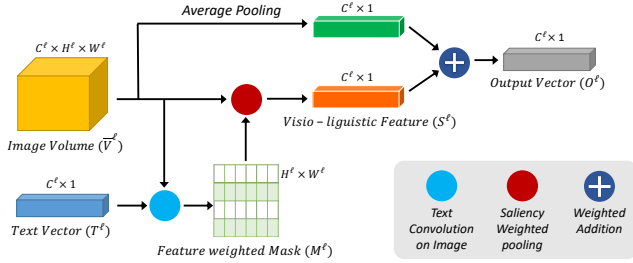


Figure 3: Visio-linguistic Pooling at ℓ^{th} level of the feature pyramid

text representation T^ℓ to obtain a *cross-modal* feature map $\mathcal{A}_{\text{cross}}^\ell \in \mathbb{R}^{H_\ell \times W_\ell}$,

$$\mathcal{A}_{\text{cross}}^\ell = \bar{V}_q^\ell \otimes T^\ell \quad (7)$$

$\mathcal{A}_{\text{cross}}^\ell$ is passed through softmax, with temperature \mathcal{T} , to obtain a feature-weightage mask M^ℓ as,

$$M^\ell = \text{softmax}\left(\frac{\mathcal{A}_{\text{cross}}^\ell}{\mathcal{T}}\right) \quad (8)$$

We provide a clear representation of the operations performed in Figure 3. We then use the obtained feature-weighted mask M^ℓ as a kernel to pool each channel in the attentional visual feature map \bar{V}_q^ℓ to generate a visio-linguistic feature $S^\ell \in \mathbb{R}^{C_\ell \times 1}$ given as,

$$S^\ell(c) = \sum_{h=1}^{H_\ell} \sum_{w=1}^{W_\ell} M^\ell(h, w) * \bar{V}_q^\ell(c, h, w) \quad (9)$$

where $1 \leq c \leq C^\ell$ and C^ℓ denotes the number of channels in the ℓ -th representation from the L levels of visual feature pyramid.

Finally, the *granular* text-conditioned visual embedding O_q^ℓ is obtained by a weighted addition of the visio-linguistic feature S^ℓ with pooled attentive visual feature map (we use the generalized-mean pooling technique **GeM** (Radenovi, Tolia, and Chum 2019) that generalizes over the max and average pooling and helps in retrieval tasks).

$$O_q^\ell = \text{Pool}(\bar{V}_q^\ell) + \beta \times S^\ell \quad (10)$$

here, β is a learnable scalar for weighting. The pooled visual embedding for the target image is also obtained as

$$O_t^\ell = \text{Pool}(V_t^\ell) \quad (11)$$

The obtained embeddings for the query image O_q^ℓ , across all the L hierarchical visual feature volumes, form the visiolinguistic feature pyramid F_q^{trans} as,

$$F_q^{\text{trans}} = \{O_q^1, \dots, O_q^\ell, \dots, O_q^L\} \quad (12)$$

Similarly, for target image we obtain the transformed feature pyramid as,

$$F_t^{\text{trans}} = \{O_t^1, \dots, O_t^\ell, \dots, O_t^L\} \quad (13)$$

3.3 HFA: Hierarchical Feature Aggregation

After obtaining the visiolinguistic feature pyramid F_q^{trans} and the feature pyramid for the target image F_t^{trans} , the next step is to aggregate them into a single feature vector for retrieval. The existing approaches use *concatenation* (used in Chen, Gong, and Bazzani (2020)), *add* or *hadamard* for aggregating the features at different levels. These operations,

by assigning equal importance to the operands, fail to capture the relative importance of the pyramidal-features and hence seem to under-perform (more details in Section 6). As convolutional networks learn features hierarchically with increasing abstraction, the embeddings in F_q^{trans} also conform to a coarse sequential structure. Hence, to obtain an efficient representation, we need an aggregation function which can learn to encapsulate the varying granularities encoded in the pyramidal features. For this, each of the features O_q^ℓ and O_t^ℓ are first linearly projected to a fixed dimensionality ($\mathbb{R}^{C_\ell \times 1} \rightarrow \mathbb{R}^{C_L \times 1}$) corresponding to the finest granularity.

$$G_q^\ell = \Omega_{\text{hfa}}^\ell(O_q^\ell), \quad G_t^\ell = \Omega_{\text{hfa}}^\ell(O_t^\ell) \quad (14)$$

We then use an LSTM module LSTM_{hfa} unrolled over L timesteps to aggregate these transformed pyramidal embeddings G_q^ℓ s into H_{hfa} followed by passing them through a BatchNormalization layer and a fully-connected layer to obtain f_{agg} . This corresponds to a *coarse* visiolinguistic representation.

$$\begin{aligned} H_{\text{hfa}} &= \text{LSTM}_{\text{hfa}}([G_q^1, \dots, G_q^L]) \\ f_{agg} &= \Omega_{\text{hfa}}(\text{BatchNorm}(H_{\text{hfa}})) \end{aligned} \quad (15)$$

We discuss the particular impact of this gated aggregation strategy in Section 6.

Similarly, to obtain the composite embedding f_{tgt} for the target image I_t , the pooled embeddings in visual feature pyramid F_t^{trans} (defined in Section 3.2) are aggregated using HFA to generate the composite embedding f_{tgt} as,

$$f_{tgt} = \text{LSTM}_{\text{hfa}}([G_t^1, \dots, G_t^L]) \quad (16)$$

3.4 VLC: Visual-Linguistic Composition

The final image-text embedding is obtained by unifying the coarse visiolinguistic representation f_{agg} with the global text representation f_{text} . First we obtain the global text representation f_{text} using a linear projection of F_{sent} into the visiolinguistic feature space.

$$f_{text} = \Omega_g(F_{sent}) \quad (17)$$

where Ω_g is a learnable linear projection layer and F_{sent} is a sentence representation introduced previously.

Then we obtain the *composed* image-text representation f_{com} (as shown in Figure 2) by residual offsetting of f_{agg} with f_{text} followed by vector normalization as,

$$f_{com} = \delta \frac{f_{agg} + f_{text}}{\|f_{agg} + f_{text}\|_2} \quad (18)$$

where δ parameter denotes the learnable normalization scale and $\|\cdot\|_2$ denotes the L_2 norm. We discuss the particular impact of this residual composition strategy in Section 6.

f_{com} , f_{tgt} and f_{text} are used as inputs to the loss functions detailed in the next section.

3.5 Loss Functions

The training dataset is characterised by 3-tuples consisting of (I_q, D_t, I_t) . Correspondingly, f_{com} represents the composed text-conditioned image embedding for (I_q, D_t) , f_{text}

represents the latent embedding for D_t and f_{tgt}^+ represents the latent embedding for I_t . Consider another image I_n sampled from the training set (I_{train}), s.t. $I_n \notin \{I_q \cup I_t\}$ where f_{tgt}^- represents its latent visual embedding which is generated using the same pipeline as for f_{tgt} . With this formalization, we next explain the combination of loss functions used to train *TRACE*.

Triplet Loss is the primary training objective which seeks to constrain the *anchor* f_{com} to align with the *target* f_{tgt}^+ by simultaneously contrasting with the embedding for a *negative* image f_{tgt}^- . The loss function is defined as

$$\mathcal{L}_{triplet} = \log(1 + e^{\|f_{com} - f_{tgt}^+\|_2} - \|f_{com} - f_{tgt}^-\|_2) \quad (19)$$

where $\|\cdot\|_2$ operator denotes the L_2 norm.

To help learn discriminative representations, we employ a hard negative strategy that interleaves the random selection of I_n with an online distance-based sampling technique. This sampling weighs $I_n \in I_{train}$ using the L_2 -distance of the corresponding embedding, f_{tgt}^- with f_{com} , with smaller distance weighted higher. Additional details are included in the supplementary material.

Discriminator Loss helps improve the alignment of f_{com} with f_{tgt} by utilizing a discriminator that penalizes distributional divergence of linear projections of these embeddings. The loss is defined as

$$\mathcal{L}_{disc} = -\mathbb{E}[\log(\mathcal{D}(f_{tgt}))] - \mathbb{E}[\log(1 - \mathcal{D}(f_{com}))] \quad (20)$$

where \mathcal{D} is the discriminator network which is trained end-to-end along with the entire model. We discuss the particular impact of using this discriminator loss in Section 6.1.

Consistency Loss constrains visual and linguistic projections of f_{com} , denoted by f_{gen}^{img} and f_{gen}^{text} , to align with latent embeddings f_{tgt} and f_{text} respectively. The objective helps regularize visual-semantic representations in the learned composed embedding f_{com} and is defined as:

$$\mathcal{L}_{cons} = \alpha_t \|f_{gen}^{text} - f_{text}\|_2 + \alpha_i \|f_{gen}^{img} - f_{tgt}\|_2 \quad (21)$$

α_t, α_i are scalar hyper-parameters and $\|\cdot\|_2$ is the L_2 norm.

In the above equation, we project the vector f_{com} using learnable transformations to obtain f_{gen}^{img} and f_{gen}^{text} as,

$$f_{gen}^{img} = \Omega_{img}^c(f_{com}) \quad f_{gen}^{text} = \Omega_{text}^c(f_{com}) \quad (22)$$

where Ω_{img}^c and Ω_{text}^c are learnable transformations of and are trained end-to-end alongside the model.

We discuss the particular impact of using this consistency loss function in Section 6.1.

Total Loss used for training is denoted by \mathcal{L}_{total} and is defined as

$$\mathcal{L}_{total} = \lambda_1 \mathcal{L}_{triplet} + \lambda_2 \mathcal{L}_{disc} + \lambda_3 \mathcal{L}_{cons} \quad (23)$$

with $\lambda_1, \lambda_2, \lambda_3$ as scalar hyperparameters.

4 Experiments

In this section, we formalize the experimental configuration including datasets, baselines, implementation details and evaluation metrics.

4.1 Datasets

We evaluate the efficacy of the proposed method, we conduct experimentation on multiple benchmark datasets. In particular, the datasets are selected to ensure maximum diversity in length of the natural language description. As indicated by Figure 4, the average number of words in the support text varies from 5 to 31.

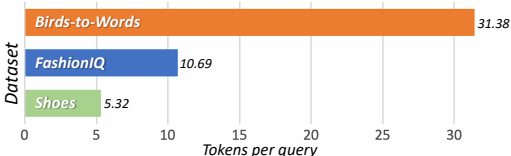


Figure 4: Average length of support text across the datasets

Shoes Shoes (Berg, Berg, and Shih 2010) is a dataset originally crawled from like.com. It is further tagged with relative captions in natural language for dialog-based interactive retrieval (Guo et al. 2018). Following (Guo et al. 2018), we use 10,000 samples for training and 4,658 samples for evaluation. This dataset is characterised by “short” natural language queries with an average text description length of 5.32 words.

FashionIQ FashionIQ (Guo et al. 2019) is a natural language-based interactive fashion product retrieval dataset. This dataset is characterized by “medium” natural language text descriptions with an average length of 10.69 words. It contains 77,684 images crawled from Amazon.com, covering three categories: Dress, Toptee, and Shirt. Among the 46,609 training images, there are 18,000 image pairs, with each pair accompanied with around two natural language sentences that describe one or multiple visual properties to modify in the reference image, such as “is darker” and “has short sleeves and is longer and more flowing”.

Birds-to-Words Birds-to-Words (Forbes et al. 2019) consists of images of birds from iNaturalist¹ combined with human-annotated paragraphs to describe the difference between these pairs of images. This dataset is characterized by “long” natural language queries with every one of 3,347 image pairs having on average 4.8 paragraphs, each describing the differences between the pair of birds in an average of 31.38 words. Birds-to-Words provides richer text descriptions in each example than any of the other datasets we study, although the number of examples is small. Forbes et al. (2019) studied the generation of these fine-grained relative captions, but we adapt their dataset for the task of retrieving described second image given the relative caption.

¹www.inaturalist.org

4.2 Baselines

We compare with the following baselines

- **Image Only** uses only image representation as composed embedding i.e. $f_{com} = f_{image}$
- **Text Only** uses only text representation as composed embedding i.e. $f_{com} = f_{text}$
- **Concat Only** concatenates (denoted by \oplus) and linear transforms the image and text representations (following details from (Vo et al. 2019)) to obtain the composed embedding i.e. $f_{com} = \text{MLP}(f_{image} \oplus f_{text})$
- **TIRG** (Vo et al. 2019) composes visual and textual representations by concatenation, followed by learning a gating connection and a residual connection to obtain composed embedding
- **VAL** (Chen, Gong, and Bazzani 2020) composes the textual representation with visual representations at multiple CNN layers using a composite transformer to obtain composed embedding.

VAL is the most recent state-of-the-art technique, and hence the strongest baseline for the purpose of our experimental study. For VAL (Chen, Gong, and Bazzani 2020) and TIRG (Vo et al. 2019) baselines, we refer to author-provided implementations with the recommended parameter settings to ensure consistency in comparison.

4.3 Implementation Details

We conduct our experiments on a machine with $4 \times$ TESLA V-100 GPU’s with 16 GB RAM using Pytorch (Paszke et al. 2019). We use Resnet-50 (He et al. 2016) (output features = 512) pre-trained on ImageNet (Deng et al. 2009) as our backbone for image encoder and a GRU (output features = 512) to encode the support text descriptions. For our experiments with pretrained text embeddings, we use BertForQuestionAnswering (Bert For Question Answering).

During training, we use the Adam (Kingma and Ba 2014)(initial learning rate= $1e^{-3}$, batch size=32) optimizer for image, text encoders and the SGD optimizer (initial learning rate= $2e^{-4}$, batch size=32) for discriminator. The learning rate was divided by 2 for the Adam optimizer and divided by 10 for the SGD optimizer when the loss plateaued on the validation set until it reached $1e^{-6}$. For the image encoder, we allow for the gradual fine-tuning by unfreezing it’s weights only after first few epochs(10 in our case) of training. We use a temperature of $\mathcal{T} = 8$. We choose the values $\lambda_1 = 1$, $\lambda_2 = 0.6$, $\lambda_3 = 0.1$ as the hyper-parameters of our loss functions. We take $\alpha_t = 1$ and $\alpha_i = 0.1$ in the consistency loss.

4.4 Evaluation Techniques

Quantitative evaluation is conducted using the Recall@K metric (R@K) which computes the percentage of evaluation queries where the target image is found within the top-K retrieved images. To ensure consistent and efficient comparison on each dataset, we report performance with $K \in \{1, 10, 50\}$ for *TRACE* compared with the other baselines.

| Method | Dress | | Toptee | | Shirt | | Average | |
|------------------------------------|--------------|--------------|--------------|--------------|--------------|--------------|--------------|--------------|
| | R@10 | R@50 | R@10 | R@50 | R@10 | R@50 | R@10 | R@50 |
| Image Only | 2.30 | 7.51 | 3.32 | 9.42 | 3.24 | 8.15 | 2.95 | 8.36 |
| Text Only | 6.39 | 20.92 | 4.60 | 15.8 | 5.94 | 21.10 | 5.64 | 19.27 |
| Concat | 7.30 | 22.31 | 5.73 | 17.87 | 7.29 | 21.31 | 6.77 | 20.50 |
| TIRG (Vo et al. 2019) | 11.11 | 29.15 | 12.95 | 30.80 | 10.20 | 25.46 | 11.42 | 28.47 |
| VAL (Chen, Gong, and Bazzani 2020) | 16.81 | 37.88 | 19.73 | 42.73 | 13.98 | 33.46 | 16.82 | 38.02 |
| <i>TRACE w/ Random Emb.</i> | 22.41 | 46.26 | 23.76 | 49.36 | 19.14 | 39.45 | 21.77 | 45.02 |
| <i>TRACE w/ BERT</i> | 22.70 | 44.91 | 24.22 | 49.80 | 20.80 | 40.80 | 22.57 | 46.19 |

Table 1: Quantitative results on Original Split of FashionIQ dataset for *TRACE w/ Random Emb* and *BERT* embeddings. Best numbers are highlighted in **bold**.

| Method | Dress | | Toptee | | Shirt | | Average | |
|------------------------------------|--------------|--------------|--------------|--------------|--------------|--------------|--------------|--------------|
| | R@10 | R@50 | R@10 | R@50 | R@10 | R@50 | R@10 | R@50 |
| Image Only | 2.92 | 10.10 | 4.53 | 11.63 | 5.34 | 14.62 | 4.26 | 12.12 |
| Text Only | 8.67 | 25.08 | 9.68 | 28.25 | 8.30 | 25.02 | 8.88 | 26.11 |
| Concat | 9.06 | 27.27 | 10.45 | 29.83 | 9.66 | 28.06 | 9.72 | 28.33 |
| TIRG (Vo et al. 2019) | 13.43 | 33.56 | 17.23 | 40.13 | 17.46 | 40.18 | 16.04 | 37.90 |
| VAL (Chen, Gong, and Bazzani 2020) | 20.87 | 43.14 | 27.03 | 52.12 | 20.90 | 46.42 | 22.90 | 47.22 |
| <i>TRACE w/ Random Emb.</i> | 26.13 | 52.10 | 31.16 | 59.05 | 26.20 | 50.93 | 27.83 | 54.02 |
| <i>TRACE w/ BERT</i> | 26.52 | 51.01 | 32.70 | 61.23 | 28.02 | 51.86 | 29.08 | 54.70 |

Table 2: Quantitative results on *VAL-Split* of the FashionIQ dataset for *TRACE* compared with existing techniques. Best numbers are highlighted in **bold**.

5 Results

In this section, we report quantitative results in Section 5.1 and qualitative results in Section 5.2 on each of the three datasets. We highlight the best numbers in **bold**.

5.1 Quantitative Results

FashionIQ Dataset Table 1 shows the quantitative performance on the evaluation set, as proposed with the benchmark in (Guo et al. 2019). As highlighted by the results in **bold**, *TRACE* significantly outperforms all existing baselines on each of the three data subsets - Dress, TopTee, Shirt by a significant margin. For instance, *TRACE* outperforms VAL by 6%, 4.5%, and 7% on the Dress, TopTee, and the Shirt subsets respectively with an average improvement of 5.7% in R@10 metric. Similarly, *TRACE* improves the results on the R@50 metric by an average of 8% across all the subsets. These results further show that our model outperforms other approaches by a substantial margin.

Discussion: The most recent baseline VAL (Chen, Gong, and Bazzani 2020) used a separate evaluation split in comparison to the original split proposed with the dataset (Guo et al. 2019). In the split used by VAL (we denote it by *VAL-Split*), a subset of the testing dataset containing only correct candidate and target images is indexed for the recall computation as part of R@K evaluation. For consistency in comparison with existing approaches and to ensure completeness in our reporting, we also evaluate the performance for all baselines on this *VAL-Split*. We report results separately for the original split in Table 1. As highlighted by the results in Table 2, *TRACE* still achieves SOTA performance by consistently outperforming all existing baselines by similar margins as in the original split.

Shoes Dataset Table 3 presents performance comparison on the shoes dataset. As highlighted in the table, *TRACE* significantly outperforms the existing techniques by a good margin. E.g., the best results from *TRACE* beat the VAL (the previous best algorithm) by at least 3% in the R@K evaluation metric.

| Method | R@1 | R@10 | R@50 |
|------------------------------------|-------------|--------------|--------------|
| Image Only | 6.07 | 25.6 | 47.87 |
| Text Only | 0.60 | 6.20 | 19.42 |
| Concat | 5.70 | 20.32 | 39.97 |
| TIRG (Vo et al. 2019) | 7.89 | 26.53 | 51.05 |
| VAL (Chen, Gong, and Bazzani 2020) | 15.44 | 47.08 | 74.74 |
| <i>TRACE w/ Random Emb.</i> | 18.11 | 52.41 | 75.42 |
| <i>TRACE w/ BERT</i> | 18.5 | 51.73 | 77.28 |

Table 3: Quantitative results on the Shoes Dataset for *TRACE w/ Random Emb* and *BERT* embeddings.

Birds-to-Words Dataset Table 4 presents the performance comparison with multiple baselines on the Birds-to-Words dataset. *TRACE* significantly outperforms the existing techniques by a significant margin. For instance, *TRACE* gives a improvement of more than 5% in R@10 evaluation metric and almost 7% in R@50 metric. This major qualitative improvements with *TRACE* also shows clearly the efficacy of *TRACE* with longer text descriptions. For VAL baseline, it was not computationally infeasible to run the author provided code because of its huge memory requirements.

We also provide results with pre-trained BERT embeddings and with Random Embeddings in Tables 3 to 2. We observe similar performance with both the embeddings



Figure 5: Qualitative results from *TRACE* compared with VAL (Chen, Gong, and Bazzani 2020). First row shows the reference image and the query text. Red box highlights the target image from the dataset.

| Method | R@10 | R@50 |
|------------------------------------|--------------|--------------|
| Image Only | 15.45 | 32.14 |
| Text Only | 1.69 | 8.34 |
| Concat | 12.05 | 34.27 |
| TIRG (Vo et al. 2019) | 15.8 | 38.65 |
| VAL (Chen, Gong, and Bazzani 2020) | - | - |
| <i>TRACE</i> w/ <i>Random Emb.</i> | 20.34 | 44.94 |
| <i>TRACE</i> w/ BERT | 19.56 | 45.24 |

Table 4: Quantitative results on Birds-to-Words dataset for *TRACE* w/ *Random Emb* and *BERT* embeddings.

with slightly better performance with BERT embeddings for Shoes and FashionIQ datasets. Overall using either embedding outperforms the existing best approaches.

5.2 Qualitative Results

To corroborate our quantitative observations, we also present extensive qualitative analysis for *TRACE*. First, in Figure 5, we present comparative visual results for *TRACE* with VAL, the strongest baseline, on the FashionIQ and Shoes datasets. We notice that our model is able to i) retrieve new images while changing certain attributes conditioned on text feedback (from Figure 5a, *TRACE* retrieves shirt which is “blue colored” with “less buttons” when VAL incorrectly retrieves “orange” colored clothes) ii) concurrently focus on global appearance and multiple local fine-grained designs (from Figure 5b, *TRACE* retrieves “shoes” that have “silver color” and “ice blue accents”).

Figure 6 presents additional qualitative results for *TRACE* on each of the three datasets. We observe that *TRACE* is able to a) retrieve new images while changing certain attributes conditioned on text feedback eg. color, material (from row 1, *TRACE* captures the “autumn-colored” while preserving the “longer” property) b) ingest multiple visual attributes and properties in the natural language text feedback (from row 2, “solid”, “black” and “orange-and-beige trim” all focus on different semantics of the image. *TRACE* captures all of the semantics in the retrieved image) c) can jointly comprehend global appearance and local details for image search (from row 2, *TRACE* captures the overall “black” look across the retrieved results and attempts to find the appropriate local variations in the design) d) aggregate multiple fine-grained semantic concepts within query sentence for image search (from row 3, *TRACE* captures the fine-grained changes like “black breast”, “green flashes” and “longer beak” in a single query and aggregates these concepts effectively).

We omit more qualitative results because of space constraints and instead provide them in Appendix A.

6 Ablation Studies

In this section, we conduct ablation studies to probe the impact of different design choices in *TRACE*. Specifically, we design independent studies for both the Network Architecture and the Loss Functions. For ease of exposition and analysis, we restrict our scope to the FashionIQ dataset and use the original evaluation, as proposed with the benchmark. Finally, we conclude the section with a short discussion on the physical significance of the recall evaluation metric in this task setting and open opportunities for future work in the domain.

Effect of Gated Feature Aggregation In *TRACE*, we aggregate the image-text representations over multiple scales to obtain a single feature vector (f_{agg}) for retrieval (refer to Equation 15). Since CNNs learn features over varying levels of abstraction, we posit that granular representations over scales exhibit a coarse sequential ordering and therefore utilize an LSTM-based operator for aggregation. To further investigate this, here we contrast with the following design choices:

- *Addition*: Vector addition for vectors in F_q^{trans} as $\sum_{l=1}^L O_l$
- *Concat*: Concatenates all $O_l \in F_q^{trans}$
- *Hadamard Product*: Performs the Hadamard Product amongst all the $O_l \in F_q^{trans}$ vectors
- *LSTM*: For each vector $O_l \in F_q^{trans}$, first perform the gating and then perform vector addition

Our observations are presented in the upper-half of Table 5. As highlighted in the results, using the LSTM based aggregation significantly outperforms all other operators. On average, we observe a gain of 6.11% on R@10 and 11.22% on R@50 over *Hadamard Product*.

Effect of Residual Offsetting In *TRACE*, f_{com} is generated by residual offsetting of f_{agg} with f_{text} which is a lin-

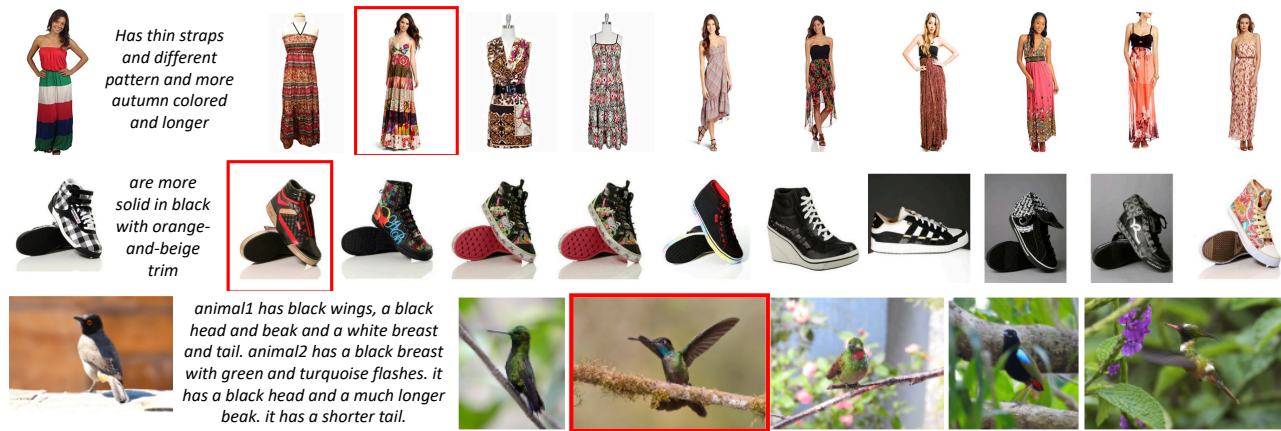


Figure 6: Qualitative results (one for each dataset) obtained from our proposed approach *TRACE*. Image in the first column denote the reference image along with the query text. Red boxes highlight the target image. Additional qualitative results are provided in Appendix A.

| Operators | | Dress | | Toptee | | Shirt | | Average | |
|------------------|---------------------|--------------|--------------|--------------|--------------|--------------|--------------|--------------|--------------|
| HFA | VLC | R@10 | R@50 | R@10 | R@50 | R@10 | R@50 | R@10 | R@50 |
| Addition | Residual Offsetting | 13.53 | 30.29 | 12.34 | 28.66 | 11.28 | 26.25 | 12.38 | 28.4 |
| Concat | Residual Offsetting | 15.46 | 34.90 | 15.91 | 37.27 | 12.70 | 30.7 | 14.69 | 34.29 |
| Hadamard Product | Residual Offsetting | 16.16 | 33.91 | 16.01 | 35.03 | 14.76 | 32.48 | 15.64 | 33.80 |
| LSTM | Residual Offsetting | 22.41 | 46.26 | 23.76 | 49.36 | 19.14 | 39.45 | 21.77 | 45.02 |
| LSTM | Concat | 19.68 | 42.89 | 19.17 | 43.65 | 15.89 | 36.75 | 18.24 | 41.09 |
| LSTM | Residual Gating | 19.28 | 42.19 | 19.88 | 45.48 | 15.94 | 37.78 | 18.33 | 41.81 |
| LSTM | Hadamard | 19.48 | 42.89 | 21.06 | 44.67 | 17.02 | 36.70 | 19.18 | 41.42 |
| LSTM | Residual Offsetting | 22.41 | 46.26 | 23.76 | 49.36 | 19.14 | 39.45 | 21.77 | 45.02 |

Table 5: Ablation study for the gated feature fusion module

| Loss Functions | Dress | | Toptee | | Shirt | | Average | |
|------------------|--------------|--------------|--------------|--------------|--------------|--------------|--------------|--------------|
| | R@10 | R@50 | R@10 | R@50 | R@10 | R@50 | R@10 | R@50 |
| Tr + Cons | 20.52 | 44.17 | 21.62 | 46.66 | 17.32 | 38.51 | 19.82 | 43.11 |
| Tr + Disc | 19.93 | 45.06 | 22.30 | 46.70 | 17.32 | 38.91 | 19.65 | 43.55 |
| Tr + Disc + Cons | 22.41 | 46.26 | 23.76 | 49.36 | 19.14 | 39.45 | 21.77 | 45.02 |

Table 6: Ablation study for the loss functions

ear projection of the sentence embedding f_{sent} . Similar visiolinguistic compositional operations have been routinely utilized in prior work (Perez et al. 2018; Vo et al. 2019; Vinyals et al. 2015). Correspondingly, we validate this design choice by contrasting with the following operators:

- *Concat*: f_{com} is obtained by linear projection of embedding generated by concatenation of f_{agg} and f_{text} .
- *Residual Gating*: f_{com} is obtained using residual gating, from the baseline (Vo et al. 2019), on f_{agg} and f_{text} .
- *Hadamard Product*: f_{com} is obtained by multiplication of f_{agg} and f_{text} .
- *Residual Offsetting*: f_{com} is obtained by residual offset of f_{agg} with f_{text} .

The results are presented in the lower-half of Table 5. As highlighted by the results, using residual operator significantly outperforms all the alternate designs. On average,

residual offsetting improves over residual gating by 2.59% at R@10 and 3.60% at R@50.

6.1 Loss Functions

Alongside the primary triplet loss objective, we additionally introduced a discriminator and a reconstruction loss to regularize the visio-linguistic representation learning. Here, we seek to study the individual impact of each of these auxiliary constraints. We present the quantitative observations in Table 6.

Effect of Discriminator Loss This loss operates between f_{com} and f_{tgt} to condition visual representations in the learned multi-modal embedding, owing to the weak training supervision. As highlighted by the results, using the \mathcal{L}_{disc} results in an average gain of 1.95% on R@10 and 1.91% on R@50.



Figure 7: On the left, we provide the query image and the corresponding textual query along with the ground truth from the FashionIQ dataset. On the right, we provide the retrieved results ranked by decreasing relevance results from our approach *TRACE*. Though the retrieved results don't contain the actual annotated sample, the results are extremely relevant to the query

Effect of Consistency Loss This loss is designed to reinforce the balanced utilization of both text and image representations in the learned multi-modal embedding. As highlighted by the results, using the \mathcal{L}_{rec} results in an average gain of 2.12% on R@10 and 1.47% on R@50.

6.2 Next Steps

The task of text-conditioned image retrieval is pertinent owing to the immense value in industry and academia. In the benchmark datasets, each input image text pair of I_q and D_t is mapped to a unique target image I_t . However, owing to the generality/ambiguity of the support text D_t , multiple indexed target images may satisfy the constraint. Thus, while the Recall metric is correct, it can be too strict to provide a coherent signal of algorithmic fitness. As highlighted by results in Figure 7, the predictions are qualitative consistent but this is not captured by the metric since the specific target image is not a part of the retrieved set. Therefore, richer annotations for benchmark datasets or working towards standardized metrics can be extremely useful.

References

- Ak, K. E.; Kassim, A. A.; Lim, J. H.; and Tham, J. Y. 2018. Learning Attribute Representations with Localization for Flexible Fashion Search. In *2018 IEEE/CVF Conference on Computer Vision and Pattern Recognition*, 7708–7717.
- Antol, S.; Agrawal, A.; Lu, J.; Mitchell, M.; Batra, D.; Zitnick, C. L.; and Parikh, D. 2015. VQA: Visual Question Answering. In *2015 IEEE International Conference on Computer Vision (ICCV)*, 2425–2433.
- Barman, A.; and Shah, S. K. 2019. A Graph-based Approach for Making Consensus-based Decisions in Image Search and Person Re-identification. *IEEE Transactions on Pattern Analysis and Machine Intelligence* 1–1.
- Bell, S.; and Bala, K. 2015. Learning Visual Similarity for Product Design with Convolutional Neural Networks. *ACM Trans. Graph.* 34(4). ISSN 0730-0301. doi:10.1145/2766959. URL <https://doi.org/10.1145/2766959>.
- Berg, T. L.; Berg, A. C.; and Shih, J. 2010. Automatic attribute discovery and characterization from noisy web data. In *European Conference on Computer Vision*, 663–676. Springer.
- Bert For Question Answering. ????. BertForQuestionAnswering. URL https://huggingface.co/transformers/model_doc/bert.html#bertforquestionanswering.
- Chen, Y.; Gong, S.; and Bazzani, L. 2020. Image Search with Text Feedback by Visiolinguistic Attention Learning. In *Proceedings of the IEEE/CVF Conference on Computer Vision and Pattern Recognition*, 3001–3011.
- Cho, K.; van Merriënboer, B.; Gulcehre, C.; Bahdanau, D.; Bougares, F.; Schwenk, H.; and Bengio, Y. 2014. Learning Phrase Representations using RNN Encoder–Decoder for Statistical Machine Translation. In *Proceedings of the 2014 Conference on Empirical Methods in Natural Language Processing (EMNLP)*, 1724–1734. Doha, Qatar: Association for Computational Linguistics. doi:10.3115/v1/D14-1179. URL <https://www.aclweb.org/anthology/D14-1179>.
- Chopra, A.; Sinha, A.; Gupta, H.; Sarkar, M.; Ayush, K.; and Krishnamurthy, B. 2019. Powering Robust Fashion Retrieval With Information Rich Feature Embeddings. In *Proceedings of the IEEE/CVF Conference on Computer Vision and Pattern Recognition (CVPR) Workshops*.
- Deng, J.; Dong, W.; Socher, R.; Li, L.-J.; Li, K.; and Fei-Fei, L. 2009. Imagenet: A large-scale hierarchical image database. In *2009 IEEE conference on computer vision and pattern recognition*, 248–255. Ieee.
- Dutta, T.; and Biswas, S. 2020. s-SBIR: Style Augmented Sketch based Image Retrieval. In *Proceedings of the IEEE/CVF Winter Conference on Applications of Computer Vision (WACV)*.
- Forbes, M.; Kaeser-Chen, C.; Sharma, P.; and Belongie, S. 2019. Neural Naturalist: Generating Fine-Grained Image Comparisons. In *Conference on Empirical Methods in Natural Language Processing (EMNLP)*. Hong Kong.
- Fu, J.; Liu, J.; Tian, H.; Li, Y.; Bao, Y.; Fang, Z.; and Lu, H. 2019. Dual attention network for scene segmentation. In *Proceedings of the IEEE Conference on Computer Vision and Pattern Recognition*, 3146–3154.
- Gao, P.; Jiang, Z.; You, H.; Lu, P.; Hoi, S.; Wang, X.; and Li, H. 2019. Dynamic Fusion With Intra- and Inter-Modality Attention Flow for Visual Question Answering. In *Proceedings of the IEEE Conference on Computer Vision and Pattern Recognition (CVPR)*, 6632–6641. doi:10.1109/CVPR.2019.00680.
- Ghosh, A.; Zhang, R.; Dokania, P. K.; Wang, O.; Efros, A. A.; Torr, P. H.; and Shechtman, E. 2019. Interactive sketch & fill: Multiclass sketch-to-image translation. In *Proceedings of the IEEE international conference on computer vision*, 1171–1180.

- Girshick, R. 2015. Fast R-CNN. In *2015 IEEE International Conference on Computer Vision (ICCV)*, 1440–1448.
- Gordo, A.; Almazán, J.; Revaud, J.; and Larlus, D. 2016. Deep image retrieval: Learning global representations for image search. In *European conference on computer vision*, 241–257. Springer.
- Guo, X.; Wu, H.; Cheng, Y.; Rennie, S.; Tesauro, G.; and Feris, R. 2018. Dialog-based Interactive Image Retrieval. In Bengio, S.; Wallach, H.; Larochelle, H.; Grauman, K.; Cesa-Bianchi, N.; and Garnett, R., eds., *Advances in Neural Information Processing Systems 31*, 678–688. Curran Associates, Inc. URL <http://papers.nips.cc/paper/7348-dialog-based-interactive-image-retrieval.pdf>.
- Guo, X.; Wu, H.; Gao, Y.; Rennie, S.; and Feris, R. 2019. Fashion IQ: A New Dataset towards Retrieving Images by Natural Language Feedback. *arXiv preprint arXiv:1905.12794*.
- Halawani, A.; Teynor, A.; Setia, L.; Brunner, G.; and Burkhardt, H. 2006. Fundamentals and Applications of Image Retrieval: An Overview. *Datenbank-Spektrum* 18: 14–23.
- Han, X.; Wu, Z.; Huang, P. X.; Zhang, X.; Zhu, M.; Li, Y.; Zhao, Y.; and Davis, L. S. 2017. Automatic spatially-aware fashion concept discovery. In *Proceedings of the IEEE International Conference on Computer Vision*, 1463–1471.
- Han, X.; Wu, Z.; Wu, Z.; Yu, R.; and Davis, L. S. 2018. VITON: An Image-Based Virtual Try-on Network. In *2018 IEEE/CVF Conference on Computer Vision and Pattern Recognition*, 7543–7552.
- He, K.; Zhang, X.; Ren, S.; and Sun, J. 2016. Deep Residual Learning for Image Recognition. In *Proceedings of the IEEE Conference on Computer Vision and Pattern Recognition (CVPR)*.
- Jandial, S.; Chopra, A.; Ayush, K.; Hemani, M.; and Krishnamurthy, B. 2019a. Robust Cloth Warping via Multi-Scale Patch Adversarial Loss for Virtual Try-On Framework. In *Proceedings of the IEEE/CVF International Conference on Computer Vision (ICCV) Workshops*.
- Jandial, S.; Chopra, A.; Ayush, K.; Hemani, M.; Krishnamurthy, B.; and Halwai, A. 2020. SieveNet: A Unified Framework for Robust Image-Based Virtual Try-On. In *The IEEE Winter Conference on Applications of Computer Vision*, 2182–2190.
- Jandial, S.; Chopra, A.; Ayush, K.; and Krishnamurthy, B. 2019b. Powering Virtual Try-On via Auxiliary Human Segmentation Learning. In *Proceedings of the IEEE/CVF International Conference on Computer Vision (ICCV) Workshops*.
- Johnson, J.; Krishna, R.; Stark, M.; Li, L.; Shamma, D. A.; Bernstein, M. S.; and Fei-Fei, L. 2015. Image retrieval using scene graphs. In *2015 IEEE Conference on Computer Vision and Pattern Recognition (CVPR)*, 3668–3678.
- Karpathy, A.; and Fei-Fei, L. 2015. Deep visual-semantic alignments for generating image descriptions. In *Proceedings of the IEEE conference on computer vision and pattern recognition*, 3128–3137.
- Kingma, D. P.; and Ba, J. 2014. Adam: A method for stochastic optimization. *arXiv preprint arXiv:1412.6980*.
- LeCun, Y.; Bengio, Y.; and Hinton, G. 2015. Deep Learning. *Nature* 521: 436–44. doi:10.1038/nature14539.
- Lee, K.-H.; Chen, X.; Hua, G.; Hu, H.; and He, X. 2018. Stacked cross attention for image-text matching. In *Proceedings of the European Conference on Computer Vision (ECCV)*, 201–216.
- Ma, J.; Pang, S.; Yang, B.; Zhu, J.; and Li, Y. 2020a. Spatial-Content Image Search in Complex Scenes. In *Proceedings of the IEEE/CVF Winter Conference on Applications of Computer Vision (WACV)*.
- Ma, Z.; Dong, J.; Long, Z.; Zhang, Y.; He, Y.; Xue, H.; and Ji, S. 2020b. Fine-Grained Fashion Similarity Learning by Attribute-Specific Embedding Network. In *Thirty-fourth AAAI Conference on Artificial Intelligence*.
- Mai, L.; Jin, H.; Lin, Z.; Fang, C.; Brandt, J.; and Liu, F. 2017. Spatial-Semantic Image Search by Visual Feature Synthesis. In *2017 IEEE Conference on Computer Vision and Pattern Recognition (CVPR)*, 1121–1130.
- McAuley, J.; Targett, C.; Shi, Q.; and Van Den Hengel, A. 2015. Image-based recommendations on styles and substitutes. In *Proceedings of the 38th international ACM SIGIR conference on research and development in information retrieval*, 43–52.
- Misra, D.; Sung, J.; Lee, K.; and Saxena, A. 2015. Tell Me Dave: Context-Sensitive Grounding of Natural Language to Manipulation Instructions. *The International Journal of Robotics Research* 35. doi:10.1177/0278364915602060.
- Noh, H.; Araujo, A.; Sim, J.; Weyand, T.; and Han, B. 2017. Large-scale image retrieval with attentive deep local features. In *Proceedings of the IEEE international conference on computer vision*, 3456–3465.
- Paszke, A.; Gross, S.; Massa, F.; Lerer, A.; Bradbury, J.; Chanan, G.; Killeen, T.; Lin, Z.; Gimelshein, N.; Antiga, L.; Desmaison, A.; Kopf, A.; Yang, E.; DeVito, Z.; Raison, M.; Tejani, A.; Chilamkurthy, S.; Steiner, B.; Fang, L.; Bai, J.; and Chintala, S. 2019. PyTorch: An Imperative Style, High-Performance Deep Learning Library. In *Advances in Neural Information Processing Systems 32*, 8024–8035. Curran Associates, Inc. URL <http://papers.neurips.cc/paper/9015-pytorch-an-imperative-style-high-performance-deep-learning-library.pdf>.
- Patro, B.; and Namboodiri, V. P. 2018. Differential Attention for Visual Question Answering. In *The IEEE Conference on Computer Vision and Pattern Recognition (CVPR)*.
- Perez, E.; Strub, F.; De Vries, H.; Dumoulin, V.; and Courville, A. 2018. Film: Visual reasoning with a general conditioning layer. In *Thirty-Second AAAI Conference on Artificial Intelligence*.
- Radenovi, F.; Tolias, G.; and Chum, O. 2019. Fine-Tuning CNN Image Retrieval with No Human Annotation. *IEEE*

- Transactions on Pattern Analysis and Machine Intelligence* 41(7): 1655–1668.
- Ramnath, S.; Saha, A.; Chakrabarti, S.; and Khapra, M. M. 2019. Scene Graph based Image Retrieval – A case study on the CLEVR Dataset.
- Ren, S.; He, K.; Girshick, R.; and Sun, J. 2015. Faster r-cnn: Towards real-time object detection with region proposal networks. In *Advances in neural information processing systems*, 91–99.
- Sangkloy, P.; Burnell, N.; Ham, C.; and Hays, J. 2016. The Sketchy Database: Learning to Retrieve Badly Drawn Bunnies. *ACM Trans. Graph.* 35(4). ISSN 0730-0301. doi: 10.1145/2897824.2925954. URL <https://doi.org/10.1145/2897824.2925954>.
- Sarafianos, N.; Xu, X.; and Kakadiaris, I. A. 2019. Adversarial Representation Learning for Text-to-Image Matching. In *Proceedings of the IEEE/CVF International Conference on Computer Vision (ICCV)*.
- Singh, A.; Natarajan, V.; Shah, M.; Jiang, Y.; Chen, X.; Batra, D.; Parikh, D.; and Rohrbach, M. 2019. Towards vqa models that can read. In *Proceedings of the IEEE Conference on Computer Vision and Pattern Recognition*, 8317–8326.
- Singhal, A.; Chopra, A.; Ayush, K.; Govind, U. P.; and Krishnamurthy, B. 2020. Towards a Unified Framework for Visual Compatibility Prediction. In *Proceedings of the IEEE/CVF Winter Conference on Applications of Computer Vision (WACV)*.
- Sinha, A.; Akilesh, B.; Sarkar, M.; and Krishnamurthy, B. 2019. Attention Based Natural Language Grounding by Navigating Virtual Environment. In *2019 IEEE Winter Conference on Applications of Computer Vision (WACV)*, 236–244.
- Tanmay, K.; and Ayush, K. 2019. Augmented reality based recommendations based on perceptual shape style compatibility with objects in the viewpoint and color compatibility with the background. In *Proceedings of the IEEE International Conference on Computer Vision Workshops*, 0–0.
- Tellex, S.; Kollar, T.; Dickerson, S.; Walter, M. R.; Banerjee, A. G.; Teller, S.; and Roy, N. 2011. Understanding natural language commands for robotic navigation and mobile manipulation. In *Twenty-fifth AAAI conference on artificial intelligence*.
- Vinyals, O.; Toshev, A.; Bengio, S.; and Erhan, D. 2015. Show and tell: A neural image caption generator. In *Proceedings of the IEEE conference on computer vision and pattern recognition*, 3156–3164.
- Vo, N.; Jiang, L.; Sun, C.; Murphy, K.; Li, L.-J.; Fei-Fei, L.; and Hays, J. 2019. Composing text and image for image retrieval-an empirical odyssey. In *Proceedings of the IEEE Conference on Computer Vision and Pattern Recognition*, 6439–6448.
- Wang, S.; Wang, R.; Yao, Z.; Shan, S.; and Chen, X. 2020. Cross-modal Scene Graph Matching for Relationship-aware Image-Text Retrieval. In *Proceedings of the IEEE/CVF Winter Conference on Applications of Computer Vision (WACV)*.
- Xu, X.; Wang, T.; Yang, Y.; Zuo, L.; Shen, F.; and Shen, H. T. 2020. Cross-Modal Attention With Semantic Consistency for Image-Text Matching. *IEEE Transactions on Neural Networks and Learning Systems* 1–14.
- Yu, A.; and Grauman, K. 2019. Thinking outside the pool: Active training image creation for relative attributes. In *Proceedings of the IEEE Conference on Computer Vision and Pattern Recognition*, 708–718.
- Yu, D.; Fu, J.; Mei, T.; and Rui, Y. 2017. Multi-level attention networks for visual question answering. In *Proceedings of the IEEE Conference on Computer Vision and Pattern Recognition*, 4709–4717.
- Yu, Q.; Liu, F.; Song, Y.-Z.; Xiang, T.; Hospedales, T. M.; and Loy, C.-C. 2016. Sketch me that shoe. In *Proceedings of the IEEE Conference on Computer Vision and Pattern Recognition*, 799–807.
- Yu, Z.; Yu, J.; Cui, Y.; Tao, D.; and Tian, Q. 2019. Deep Modular Co-Attention Networks for Visual Question Answering. In *Proceedings of the IEEE Conference on Computer Vision and Pattern Recognition (CVPR)*, 6281–6290.
- Zeiler, M. D.; and Fergus, R. 2014. Visualizing and Understanding Convolutional Networks. In Fleet, D.; Pajdla, T.; Schiele, B.; and Tuytelaars, T., eds., *Computer Vision – ECCV 2014*, 818–833. Cham: Springer International Publishing. ISBN 978-3-319-10590-1.
- Zhang, H.; Goodfellow, I.; Metaxas, D.; and Odena, A. 2019. Self-attention generative adversarial networks. In *International Conference on Machine Learning*, 7354–7363.
- Zhang, Q.; Lei, Z.; Zhang, Z.; and Li, S. Z. 2020. Context-Aware Attention Network for Image-Text Retrieval. In *Proceedings of the IEEE/CVF Conference on Computer Vision and Pattern Recognition (CVPR)*.
- Zhao, B.; Feng, J.; Wu, X.; and Yan, S. 2017. Memory-Augmented Attribute Manipulation Networks for Interactive Fashion Search. In *2017 IEEE Conference on Computer Vision and Pattern Recognition (CVPR)*, 6156–6164.
- Zhou, F.; and Lin, Y. 2016. Fine-grained image classification by exploring bipartite-graph labels. In *Proceedings of the IEEE Conference on Computer Vision and Pattern Recognition*, 1124–1133.

A Additional Results



Figure 8: Additional Qualitative results on the FashionIQ-Shoes dataset